Stable acidic water oxidation with a cobalt-iron-lead oxide catalyst operating *via* a cobalt-selective self-healing mechanism

Darcy Simondson[a], Manjunath Chatti[a]*, Shannon A. Bonke[b], Marc F. Tesch[b], Ronny Golnak[c], Jie Xiao[c], Dijon A. Hoogeveen[a], Pavel V. Cherepanov[a], James L. Gardiner[a], Antonio Tricoli[d], Douglas R. MacFarlane[a,e]*, Alexandr N. Simonov[a,e]*

[a] Mr. D. Simondson, Dr. M. Chatti, Dr. D. A. Hoogeveen, Dr. P. V. Cherepanov, Mr. J. L. Gardiner, Prof. D. R. MacFarlane, Dr. A. N. Simonov
School of Chemistry
Monash University
Clayton, Victoria 3800, Australia
E-mail: manjunath.chatti1@monash.edu
E-mail: douglas.macfarlane@monash.edu
E-mail: alexandr.simonov@monash.edu

[b] Dr. S. A. Bonke, Dr. M. F. Tesch
Max Planck Institute for Chemical Energy Conversion
45470 Mülheim an der Ruhr, Germany

[c] Dr. R. Golnak, Dr. J. Xiao
Helmholtz-Zentrum Berlin für Materialien und Energie
12489 Berlin, Germany

[d] Prof. A. Tricoli
Nanotechnology Research Laboratory, Faculty of Engineering
The University of Sydney
Sydney, NSW 2006 Australia

[e] Prof. D. R. MacFarlane, Dr. A. N. Simonov
ARC Centre of Excellence for Electromaterials Science, Monash University
Clayton, Victoria 3800, Australia

Abstract: The instability and expense of anodes for water electrolyzers with acidic electrolytes can be overcome through the implementation of the cobalt-iron-lead oxide electrocatalyst, [Co-Fe-Pb]O_x, that is self-healing in the presence of dissolved metal precursors. However, the latter requirement is pernicious for the membrane and especially the cathode half-reaction since Pb^{2+} and Fe^{3+} precursors poison the state-of-the-art platinum H_2 evolving catalyst. To address this, we demonstrate the invariably stable operation of [Co-Fe-Pb]O_x in acidic solutions through a cobalt-selective self-healing mechanism without the addition of Pb^{2+} and Fe^{3+} and investigate the kinetics of the process. Soft X-ray absorption spectroscopy reveals that low concentrations of Co^{2+} in the solution stabilize the catalytically active Co(Fe) sites. The highly promising performance of this system is showcased by steady water electrooxidation at 80 °C and 10 mA cm^{-2}, using a flat electrode, at an overpotential of 0.56 ± 0.01 V on a one-week timescale.

Dominance of renewably generated electricity and the alleviation of fossil fuel reliance within global energy markets will require efficacious storage solutions that address the sporadic nature of abundant solar and wind energy.[1] Renewably generated H_2 is capable of becoming a primary energy vector and storage solution for energy infrastructures, as well as an intermediate to other sustainable synthetic fuels and chemicals.[2] Of the viable methods for H_2 production, water electrolysis paired with renewable energy technologies is highly promising in terms of the abundance of water supplies and the zero-carbon circularity of the overall process.[3]

Acidic water electrolysis with a polymer electrolyte membrane (PEM) presents a range of technological advantages as compared to other modes of H_2O splitting; this makes low pH PEM water electrolyzers capable of sustainable hydrogen production at the TW scale.[4] However, the most stable and active catalysts for the anodic water electrooxidation, *viz.* the oxygen evolution reaction (OER), under acidic conditions are oxides based on the prohibitively scarce and costly iridium and ruthenium. Moreover, even these catalysts do not avoid issues of eventual degradation under ambient conditions,[5] processes that become even worse at the elevated temperatures of an operating PEM electrolyser.[6] Thus, even the most stable water oxidation electrocatalysts undergo some degree of corrosion under low pH conditions and likely attain a quasi-equilibrium with the resulting dissolved species during the OER,[7] which sustains their operation on a reasonable timescale. Building upon this hypothesis, a dynamically stable catalytic system where dissolved precursors are intentionally added to the electrolyzed solutions can be designed. This was recently demonstrated under acidic conditions through the introduction of self-healing Pd-based catalysts,[8] and in particular the cobalt-iron-lead oxide system (reactions 1-2), which catalytic activity is majorly defined by cobalt, high stability is provided by the PbO_2 matrix, and the iron precursor facilitates *in situ* electrodeposition.[9] This [Co-Fe-Pb]O_x catalyst operates with no losses in activity with an OER faradaic efficiency of 99 ± 2% on a week-long timescale at pH below 1 and temperatures up to 80 °C.[9] Theoretically, this performance can last indefinitely.

$$a\mathrm{Co}^{2-}_{(sol)} + b\mathrm{Fe}^{3-}_{(sol)} + c\mathrm{Pb}^{2+}_{(sol)} + x\mathrm{H_2O} \rightleftarrows \rightleftarrows \left[\mathrm{Co}^{\geq 3+}_{a}\mathrm{Fe}^{\geq 3+}_{b}\mathrm{Pb}^{\geq 4+}_{c}\right]\mathrm{O}_x + 2x\mathrm{H}^+ + y\mathrm{e}^- \quad (1)$$

$$2\mathrm{H_2O} \xrightarrow{[\text{Co-Fe-Pb}]O_x} \mathrm{O_2} + 4\mathrm{H}^+ + 4\mathrm{e}^- \quad (2)$$

A limitation of the presence of the dissolved metal cations in the anode solution, either formed due to the catalyst corrosion or added intentionally, is their potential interference with the proton exchange electrolyte and especially with the hydrogen evolving cathode.[10] If the potential of the latter is negative enough, the catalytically active surface will be rapidly poisoned by electrodeposition of unwanted metals from the cations migrating through the electrolyte. Partial cathode poisoning can occur even with ruthenium and iridium, which are substantially less active towards the hydrogen evolution reaction (HER) than platinum.[11] Significant deactivation of a Pt catalyst can occur if cations of non-noble metals from the edges of the hydrogen volcano plot reach the cathode. This is exemplified in Figure S1 and discussion therewith for the Fe^{3+} and Pb^{2+} precursors of the [Co-Fe-Pb]O_x catalyst, which undergo underpotential deposition[12] on platinum and thereby poison it. Contrasting this behavior, no detrimental effects of the presence of Co^{2+} on the voltammetric profile and the HER activity of Pt at −0.100 V *vs.* RHE was found (Figure S1).

Thus, among precursors that sustain stable operation of the self-healing [Co-Fe-Pb]O_x catalytic system, only Co^{2+} is benign with respect to the cathode. Exclusion of Fe^{3+} from the electrooxidised solution should be possible as it would only affect the initial rate of catalyst electrodeposition, but not its steady-state activity.[9] In principle, replacement of platinum with a non-noble metal H_2 evolving catalyst like MoS_2[13] can also be considered, as this would likely mitigate the problem of underpotential deposition. On the downside, this would also shift the cathode potential to more negative values and thereby induce overpotential deposition of the HER-inactive lead. Therefore, the concentration of dissolved Pb^{2+} cations should be kept as low as possible. However, this requires the [Co-Fe-Pb]O_x system to demonstrate similarly high stability without the addition of dissolved Pb^{2+}, which is a precursor to the acid-stable PbO_2 matrix that accommodates and stabilizes the catalytically active Co(Fe) sites.[9] The present study aims to establish such a mode of operation for the [Co-Fe-Pb]O_x catalyst during the electrooxidation of water at low pH and elevated temperatures in the absence of Pb^{2+} and Fe^{3+} precursors. Performance of the [Co-Fe-Pb]O_x catalyst provided by the previously optimized precursor composition, *viz.* 5 mM Co^{2+} + 1 mM Fe^{3+} + 0.5 mM Pb^{2+},[9] was considered as the benchmark. This mixture was also used herein for the electrodeposition of catalyst films onto either glass slides coated with F-doped SnO_2 (FTO), platinized titanium screen grid (Pt-Ti), or Sb:SnO_2-coated titanium substrates for subsequent testing (see Experimental for extended details). The deposition time for the key stability experiments was limited to 1 h to produce comparatively thin films (Figure S2), which minimizes the amount of metals that could dissolve into the electrolyte solutions and facilitate self-healing of the catalysts *via* reaction 1.

Operating the [Co-Fe-Pb]O_x catalyst in the nominally pure 0.1 M H_2SO_4 solution resulted in a rapid deterioration of the performance, in particular during galvanostatic tests at 10 mA cm^{-2} (all current densities are reported normalized to the geometric surface area of the electrodes) (Figure 1a). However, exclusion of Fe^{3+} and Pb^{2+} while retaining the 5 mM Co^{2+} precursor in the electrooxidised solutions restored stable operation of [Co-Fe-Pb]O_x. Under these conditions, the OER overpotential required to maintain the reaction rate of 10 mA cm^{-2} (η_{10}) was only 0.014 ± 0.004 V higher than that established after 1 h of deposition in the presence of all three metal precursors (Figure 1b). This behavior was also found to be essentially independent of the initial amount and properties of [Co-Fe-Pb]O_x (Figures S2 and S3 and discussion therewith), confirming that the increased loadings and initial morphology are not critical for the stable operation. Under more challenging reaction conditions, *viz.* at temperature elevated to 60 °C and pH decreased to 0, the cobalt-selective self-healing mechanism was still sufficient to sustain robust operation of the [Co-Fe-Pb]O_x catalytic system (Figure 1c).

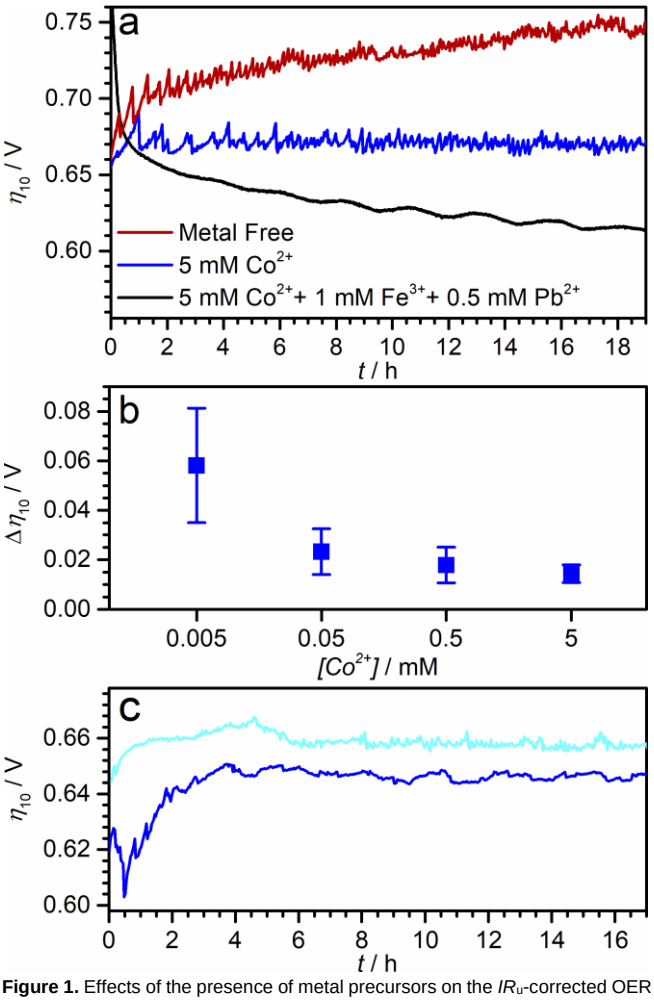

Figure 1. Effects of the presence of metal precursors on the IR_u-corrected OER overpotential at 10 mA cm^{-2} (η_{10}) sustained by the [Co-Fe-Pb]O_x/FTO catalyst: (a) chronopotentiograms in 0.1 M H_2SO_4 at 23 ± 2 °C collected with 5 mM Co^{2+} precursor only (*blue*) compared to the data obtained with no precursors added (*red*) and in the presence of 5 mM Co^{2+} + 1 mM Fe^{3+} + 0.5 mM Pb^{2+} (*black*); (b) change in the quasi-stabilized potential at 20 h in the presence of different concentrations of Co^{2+} only with respect to that established after 1 h deposition from 5 mM Co^{2+} + 1 mM Fe^{3+} + 0.5 mM Pb^{2+} in 0.1 M H_2SO_4 at 23 ± 2 °C (data are shown as mean ± standard deviation derived from testing three independent electrodes under each set of conditions); (c) chronopotentiograms recorded in the presence of 5 mM Co^{2+} only in 0.1 (*blue*) and 1 M H_2SO_4 (*teal*) at 60 °C.

The effect of the modified electrolysis solution on the electronic structure of the [Co-Fe-Pb]O_x catalysts films was explored by soft X-ray absorption spectroscopy (XAS). Spectra of the Co and Fe $L_{2,3}$-edges (2*p* to 3*d* transitions) for the catalyst as deposited from the original three-metal solution indicate that both cobalt and iron are primarily in the cobaltic/ferric oxidation state, with comparable structural motifs to reference materials $LiCoO_2$ and CoOOH, and $LiFeO_2$ and FeOOH, respectively (Figure 2a-b). Meanwhile, the O K-edge spectra show a shape change from that of pure PbO_2 (Figure 2c), reflecting additional contributions from O bound to Co and Fe, as it would be expected for the Co/Fe doping into the lead(IV) oxide lattice.[9]

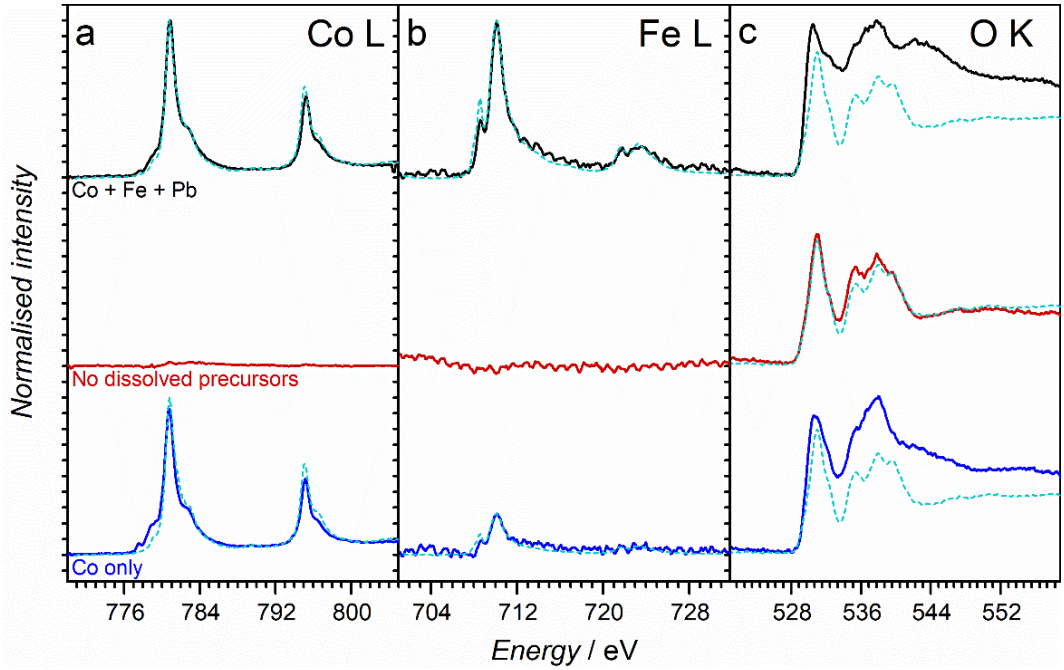

Figure 2. X-ray absorption spectra collected at the (a) Co $L_{2,3}$, (b) Fe $L_{2,3}$ and (c) O K-edges for the [Co-Fe-Pb]O_x catalyst films after 2 h deposition from 5 mM Co^{2+} + 1 mM Fe^{3+} + 0.5 mM Pb^{2+} (*black*), and similarly deposited films after operation for 20 h with no metal precursors present (*red*) and with only 5 mM Co^{2+} added to the electrolyzed solution (*blue*). *Dashed teal* curves show data for the (a) $LiCoO_2$, (b) $LiFeO_2$ and (c) PbO_2 reference materials. Electrochemical tests used 0.1 M H_2SO_4 as a supporting electrolyte and were undertaken at 10 mA cm^{-2} and 23 ± 2 °C.

Operation of the [Co-Fe-Pb]O_x catalyst in the absence of added precursors strongly suppressed the intensity of the Co signals (Figure 2a), resulted in an essentially featureless Fe spectrum (Figure 2b), and produced an O K-edge spectrum closely resembling that of pure PbO_2 (Figure 2c). These observations indicate the significant loss of the catalytically more active Co(Fe) species, in agreement with the electrochemical data (Figure 1a). In stark contrast, operation in the solution containing only Co^{2+} resulted in a strong signal at the Co $L_{2,3}$-edges, comparable to that from testing in the presence of all metal precursors. The spectrum exhibits a slightly more intense low-energy shoulder at the Co L_3-edge but is of almost equal intensity to the original one (Figure S4), suggesting no significant additional deposition of cobalt oxides on the catalyst surface. XAS of the fresh catalyst deposited from the Co^{2+} + Fe^{3+} + Pb^{2+} mixture indicates approximately six-fold lower intensity at the Fe L-edge compared to the Co L-edge (Figure S4), which is in close agreement with the initial precursor ratio of 5 : 1. When operating the catalyst in the presence of Co^{2+} only, an Fe L-edge signal was again detected, with a decreased intensity but essentially the same spectral shape as in the as-deposited [Co-Fe-Pb]O_x (Figure 2). The O K-edge spectra of the two samples were largely consistent. Finally, comparison of the X-ray photoelectron spectra of the catalyst before and after the OER test in the presence of the cobalt precursor only corroborates that such operating conditions induce no significant changes to the electronic states of the metals and the surface composition (Figure S5). Taken together, XAS and XPS indicate that the dominant structural motifs in the catalyst are essentially unchanged by operation in the presence of the Co^{2+} precursor only compared to those of the original material formed in solutions that contain all three precursors. Consequently, it appears that the mode of the catalytic operation of [Co-Fe-Pb]O_x is unaffected by the intentional additions of Pb^{2+} and Fe^{3+}.

The capability of the cobalt-iron-lead oxide catalyst to operate without the addition of either Pb^{2+} or Fe^{3+} to the electrolyzed solution prompted further investigation into the effects of the Co^{2+} concentration on the performance. Decreasing the amount of the of cobalt(II) precursor induced a slow positive shift of the potential during galvanostatic tests, however this always eventuated in quasi-stabilization over less than 4 h, even when only 0.005 mM Co^{2+} was added (Figure S6). The η_{10} measured in the presence of progressively decreasing Co^{2+} concentrations slightly increased with respect to that measured after 20 h in the presence of all precursors, but this loss in performance was still not very significant and less than 0.025 V for 0.05 mM (Figure 1b). Hence, it was concluded that 0.05 mM of Co^{2+} provides a reasonable compromise between the intention to minimize the precursor concentration and the associated losses in performance.

Analysis of the [Co-Fe-Pb]O_x composition was undertaken before and after water oxidation tests in the presence of 0.05 mM Co^{2+} to examine the equilibrium between dissolution and deposition (Table 1). Following 24 h operation at ambient temperature, a detectable corrosion of all metals into the electrooxidised solution was expectedly observed and the resulting composition can be considered as the actual active state of the catalyst. Partial loss of cobalt is explained by the 100-fold lower concentration of the Co^{2+} precursor during the catalytic tests as compared to those used for electrodeposition (5 mM Co^{2+}). The amount of lead released into the solution during the OER reflects the concentration of dissolved Pb^{2+} required to maintain the system in equilibrium. This concentration was measured herein to be not higher than the very low value of approximately 2 µM.

Table 1. Concentrations (μmol cm^{-2})[a] of Co, Fe and Pb in the [Co-Fe-Pb]O_x catalyst films before[b] and after[c] OER tests.

Time / h	23 ± 2 °C			80 °C		
	Co	Fe	Pb	Co	Fe	Pb
0	9.9	0.7	50	12	8.3	49
24	4.3	0.3	38	10	4.1	39
160	Not analyzed			4.5	3.1	37

[a] Measured by inductively coupled plasma optical emission spectroscopic (ICP-OES) analysis of the solutions derived from digesting the catalyst layers. [b] Materials were synthesized on Pt-Ti electrodes by galvanostatic oxidation (10 mA cm^{-2}) of 0.1 M H_2SO_4 containing 0.5 mM Pb^{2+}, 5 mM Co^{2+} and 1 mM Fe^{3+} at corresponding temperature for 1 h. [c] Galvanostatic oxidation (10 mA cm^{-2}) of 0.1 M H_2SO_4 containing 0.05 mM Co^{2+} at corresponding temperature.

Overall, the results presented above suggest a key catalytic role of cobalt within the multicomponent [Co-Fe-Pb]O_x catalyst, although the stabilizing effect of the Co^{2+} precursor on iron within the material is also notable (Figure 2b). Most importantly, the presented data attest to the capability of the system to operate through a selective self-healing of the key "Co(Fe)O_y" motif (reaction 3) at relatively low concentrations of Co^{2+}.

$$n\mathrm{Co}^{2+}_{(sol)} + x\mathrm{H_2O} + \left[\mathrm{Co}^{\geq 3+}_{a-n}\mathrm{Fe}^{\geq 3+}_{b}\mathrm{Pb}^{\geq 4+}_{c}\right]\mathrm{O}_{x-m} \rightleftarrows$$
$$\rightleftarrows \left[\mathrm{Co}^{\geq 3+}_{a}\mathrm{Fe}^{\geq 3+}_{b}\mathrm{Pb}^{\geq 4+}_{c}\right]\mathrm{O}_{x} + 2x\mathrm{H}^{+} + pe^{-} \qquad (3)$$

It is additionally noted that water oxidation in the presence of Co^{2+} only, using unmodified FTO electrodes, requires significantly more positive potentials than with [Co-Fe-Pb]O_x (Figure S7). This indicates that the lead(IV) oxide matrix favorably shifts the equilibrium of the electrodeposition/dissolution of the catalytic cobalt oxide species, which enables more stable deposition at less positive potentials. The PbO_2 component itself was found to require only a very low, μM-level concentration of lead in the solution to maintain the integrity of the catalyst, indicating that the equilibrium of reaction 1 is highly favorably shifted towards fully oxidized, solid-state [Co-Fe-Pb]O_x.

Thus, reactions 2 and 3 define the kinetics of water oxidation catalyzed by the [Co-Fe-Pb]O_x system, which we aimed to investigate further as a function of temperature using more stable platinized titanium grid (Pt-Ti) substrates (note that this change did not affect the intrinsic performance of the catalyst; see Figure S7 and attached comments). Following the deposition for 1 hour at various temperatures (see Figure S8 and attached comments), the activity of [Co-Fe-Pb]O_x in the presence of 0.05 mM Co^{2+} was tested in both galvanostatic (Figure 3a) and potentiostatic (Figure S9) modes to construct the OER polarization plots at four temperatures (Figure 3b). These semilogarithmic plots demonstrated close to linear dependence, with corresponding η *vs.* log j (Tafel) slopes increasing with temperature, as expected from the Butler-Volmer theory. These slopes are often used in the literature to interpret the nature of the rate-determining step, though this approach should be applied with caution when considering the complex OER mechanism.[14] Therefore, it is conservatively noted herein that the η *vs.* log j slopes measured for [Co-Fe-Pb]O_x operating in the presence of 0.05 mM Co^{2+} (0.07-0.09 V dec^{-1}) are closely comparable to those reported for the conventional noble (0.04-0.07 V dec^{-1})[15] and non-noble-metal (0.05-0.09 V dec^{-1})[16] based OER catalysts. The activation energy of 62 ± 6 kJ mol^{-1} determined herein at the overpotential of 0.55 V also falls within the range typically reported for the OER at low pH catalyzed by iridium-based (*e.g.* 37-52 kJ mol^{-1}),[17] PbO_2 (*e.g.* 50-100 kJ mol^{-1})[18] and other oxides. These findings can be interpreted as an indication of similar modes of the catalytic operation by [Co-Fe-Pb]O_x and other oxide materials, thus implying that the effects of self-healing (reaction 3) on the OER kinetics are not significant and/or are very similar for these catalysts.

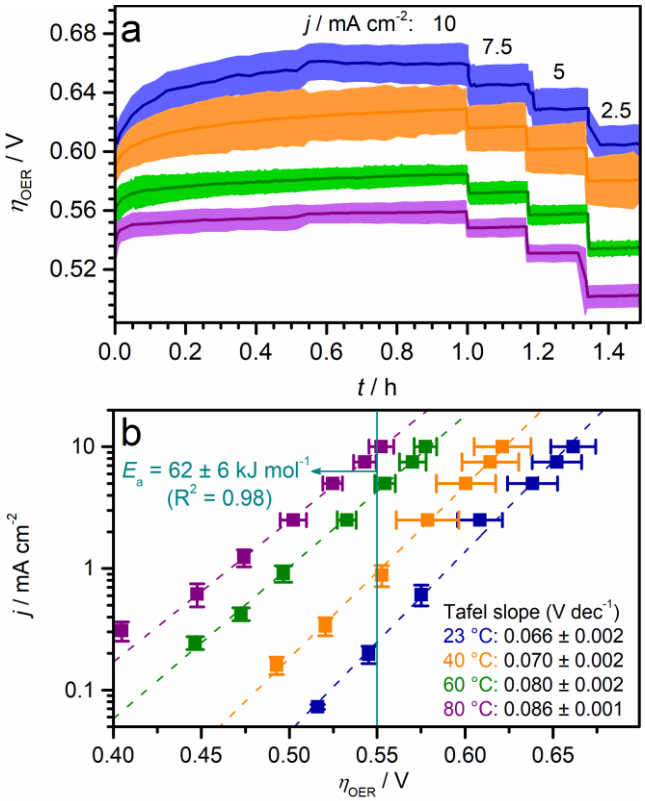

Figure 3. Effects of temperature (23 ± 2 °C – *blue*, 40 °C – *green*, 60 °C – *orange*, 80 °C – *purple*) on the OER catalytic activity of [Co-Fe-Pb]O_x in 0.05 mM Co^{2+} + 0.1 M H_2SO_4. (a) IR_u-free chronopotentiograms recorded consecutively at 10, 7.5, 5 and 2.5 mA cm^{-2} (curves show average and shadings show one standard deviation for 3 independent tests). (b) Quasi-steady state OER polarization plots derived from galvano- and potentiostatic measurements and presented as mean ± standard deviation (3 independent experiments under each set of conditions) on an IR_u-free overpotential scale; dashed lines show linear fits from which Tafel slopes and standard error were derived using a 95% confidence interval, while solid *teal* line shows η = 0.55 V used to calculate the activation energy (R^2 corresponds to a linear fit to the Arrhenius plot). Catalysts were deposited from 5 mM Co^{2+} + 1 mM Fe^{3+} + 0.5 mM Pb^{2+} solutions in 0.1 M H_2SO_4 for 1 h at 10 mA cm^{-2} at corresponding temperature.

A highly notable attribute of the [Co-Fe-Pb]O_x catalyst operating with all dissolved metal precursors added to the solution is in its ability to sustain the OER for at least one week at 80 °C,[9] which is also demonstrated herein when only including 0.05 mM Co^{2+} (Figure 4a). Critically, following an initial period of equilibration, the system exhibited an OER overpotential of *ca* 0.56-0.57 V at the rate of 10 mA cm^{-2} that remained stable over one week. Furthermore, the stabilized concentrations of cobalt and lead on the electrode surface in this experiment were very similar to those after the short-term tests under ambient conditions (Table 1). Collectively, this establishes that the [Co-Fe-Pb]O_x catalyst is capable of long-term operation for the electrooxidation of water at low pH and elevated temperatures through a cobalt-selective self-healing mechanism that provides intrinsic stability.

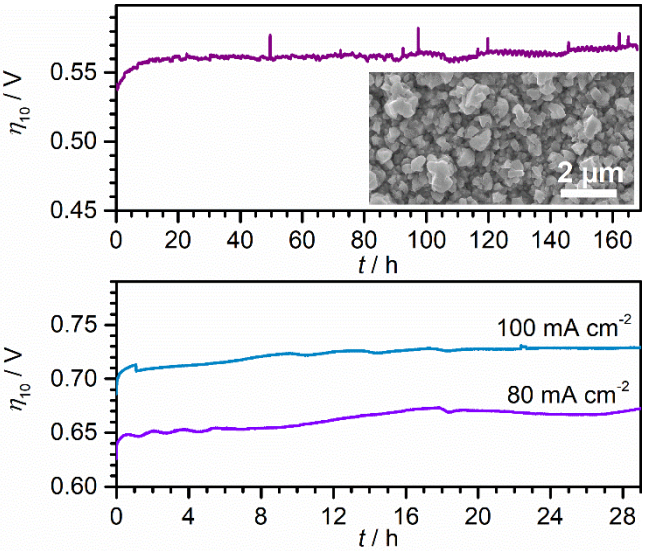

Figure 4. (a) Long-term galvanostatic oxidation (10 mA cm^{-2}) of quiescent 0.1 M H_2SO_4 containing 0.05 mM Co^{2+} catalyzed by [Co-Fe-Pb]O_x supported on a Pt-Ti substrate at 80 °C; inset displays a scanning electron micrograph of the resultant catalyst morphology post 168 h test. (b) Long-term galvanostatic oxidation of quiescent 0.5 M H_2SO_4 containing 5 mM Co^{2+} at 23 ± 2 °C catalyzed by [Co-Fe-Pb]O_x supported on a Pt-Ti substrate at 100 mA cm^{-2} (*navy*) and on a [SbSn]O_x/Ti substrate at 80 mA cm^{-2} (*purple*). Catalysts were deposited from 5 mM Co^{2+} + 1 mM Fe^{3+} + 0.5 mM Pb^{2+} solutions in 0.1 M H_2SO_4 for 1 h at 10 mA cm^{-2} at corresponding temperature.

Another feature of the self-healing [Co-Fe-Pb]O_x system are the relatively high current densities achievable with this catalyst even when fabricated as flat electrodes,[9] which is also demonstrated herein for operation at 80-100 mA cm^{-2} in the presence of the Co^{2+} precursor only (Figure 4b). Albeit with slightly longer equilibration times, the cobalt-selective mode enables stable operation under these conditions, even with nominally flat catalyst films. Moreover, some of these experiments were undertaken using titanium electrodes functionalized with Sb-doped SnO_2 (ATO), rather than platinum, to further highlight the favorable characteristics of the [Co-Fe-Pb]O_x system. ATO is a well-established stable electrocatalyst support that can be prepared in a variety of morphologies including as high surface area materials,[19] as required for the fabrication of water electrolyser anodes, for which integration of [Co-Fe-Pb]O_x remains a promising landmark towards industrial application.

In summary, the present work highlights a significant step forward in the applicability of the self-healing OER [Co-Fe-Pb]O_x electrocatalyst for acidic water electrolysis, *viz.* exclusion of the pernicious lead(II) and iron(III) precursors and 100-fold decrease in the amount of cobalt(II) precursor in the electrolyzed solution with minimal losses in performance. While the catalytic activity demonstrated herein is among the highest for the noble-metal free materials, it is still lower than that of the Ru- and Ir-based systems.[16a, 20] Given the low cost of the components, increased loadings of [Co-Fe-Pb]O_x at the anodes can partially address this limitation, although further improvements in the activity are still desirable. Most importantly, contrasting many other low-pH OER catalysts which ubiquitously suffer irreversible degradation at ambient temperature, the [Co-Fe-Pb]O_x system operating in the presence of small amounts of the intentionally added cobalt precursor demonstrates outstanding stability even at 80 °C. Thus, it is a key step in the endeavor towards integration of this catalytic system into low pH electrolyzer designs.

Experimental Section

Experimental Details are provided in Supporting Information

Acknowledgements

Part of this work was undertaken using the facilities at BESSY II Synchrotron (Berlin, Germany) and Monash Centre for Electron Microscopy (Australia). The authors are grateful for the financial support of this work by the Australian Renewable Energy Agency (ARENA, contract No. 2018/RND008) and Australian Research Council (Centre of Excellence for Electromaterials Science, CE140100012; Future Fellowship to ANS, FT200100317), as well as to Dr. Thomas R. Gengenbach from CSIRO (Clayton, Australia) for his generous help with the collection and analysis of the XPS data. DS acknowledges the support and contribution provided by the Russell and Jenny Tait Postgraduate Research Scholarship.

Keywords: heterogeneous catalysis • electrochemistry • kinetics • hydrogen • electronic structure

[1] a) R. Wiser, K. Jenni, J. Seel, E. Baker, M. Hand, E. Lantz, A. Smith, *Nature Energy* **2016**, *1*, 1-8; b) E. L. González, F. I. Llerena, M. S. Pérez, F. R. Iglesias, J. G. Macho, *International Journal of Hydrogen Energy* **2015**, *40*, 5518-5525; c) P. Denholm, E. Ela, B. Kirby, M. Milligan *Role of energy storage with renewable electricity generation*; National Renewable Energy Lab.(NREL), Golden, CO (United States): 2010. ; d) A. Castillo, D. F. Gayme, *Energy Conversion and Management* **2014**, *87*, 885-894.

[2] a) M. Ewing, B. Israel, T. Jutt, H. Talebian, L. Stepanik, **2020**; b) D. R. MacFarlane, J. Choi, B. H. Suryanto, R. Jalili, M. Chatti, L. M. Azofra, A. N. Simonov, *Advanced Materials* **2020**, *32*, 1904804; c) D. R. MacFarlane, P. V. Cherepanov, J. Choi, B. H. Suryanto, R. Y. Hodgetts, J. M. Bakker, F. M. F. Vallana, A. N. Simonov, *Joule* **2020**.

[3] a) C. M. Liu, N. K. Sandhu, S. T. McCoy, J. A. Bergerson, *Sustainable Energy & Fuels* **2020**, *4*, 3129-3142; b) S. Grigoriev, V. Fateev, D. Bessarabov, P. Millet, *International Journal of Hydrogen Energy* **2020**, *45*, 26036-26058.

[4] a) S. Park, Y. Shao, J. Liu, Y. Wang, *Energy & Environmental Science* **2012**, *5*, 9331-9344; b) T. Reier, H. N. Nong, D. Teschner, R. Schlögl, P. Strasser, *Advanced Energy Materials* **2017**, *7*, 1601275.

[5] a) S. Geiger, O. Kasian, M. Ledendecker, E. Pizzutilo, A. M. Mingers, W. T. Fu, O. Diaz-Morales, Z. Li, T. Oellers, L. Fruchter, *Nature Catalysis* **2018**, *1*, 508-515; b) O. Kasian, J. P. Grote, S. Geiger, S. Cherevko, K. J. Mayrhofer, *Angewandte Chemie International Edition* **2018**, *57*, 2488-2491; c) O. Kasian, S. Geiger, T. Li, J.-P. Grote, K. Schweinar, S. Zhang, C. Scheu, D. Raabe, S. Cherevko, B. Gault, *Energy & Environmental Science* **2019**, *12*, 3548-3555.

[6] a) L. Liu, W. Chen, Y. Li, *Journal of Membrane Science* **2016**, *504*, 1-9; b) O. Schmidt, A. Gambhir, I. Staffell, A. Hawkes, J. Nelson, S. Few, *International Journal of Hydrogen Energy* **2017**, *42*, 30470-30492.

[7] a) S. Ardizzone, G. Fregonara, S. Trasatti, *Electrochimica Acta* **1990**, *35*, 263-267; b) S. H. Chang, N. Danilovic, K.-C. Chang, R. Subbaraman, A. P. Paulikas, D. D. Fong, M. J. Highland, P. M. Baldo, V. R. Stamenkovic, J. W. Freeland, *Nature communications* **2014**, *5*, 1-9; c) R. Zhang, N. Dubouis, M. Ben Osman, W. Yin, M. T. Sougrati, D. A. Corte, D. Giaume, A. Grimaud, *Angewandte Chemie International Edition* **2019**, *58*, 4571-4575; d) K. Sardar, E. Petrucco, C. I. Hiley, J. D. Sharman, P. P. Wells, A. E. Russell, R. J. Kashtiban, J. Sloan, R. I. Walton, *Angewandte Chemie* **2014**, *126*, 11140-11144; e) F. Claudel, L. Dubau, G. Berthomé, L. Sola-Hernandez, C. Beauger, L. Piccolo, F. Maillard, *ACS Catalysis* **2019**, *9*, 4688-4698; f) V. Pfeifer, T. E. Jones, J. J. V. Vélez, R. Arrigo, S. Piccinin, M. Hävecker, A. Knop-Gericke, R. Schlögl, *Chemical science*

2017, *8*, 2143-2149; g) T. Binninger, R. Mohamed, K. Waltar, E. Fabbri, P. Levecque, R. Kötz, T. J. Schmidt, *Scientific reports* **2015**, *5*, 1-7; h) P. Lettenmeier, J. Majchel, L. Wang, V. Saveleva, S. Zafeiratos, E. Savinova, J.-J. Gallet, F. Bournel, A. Gago, K. A. Friedrich, *Chemical science* **2018**, *9*, 3570-3579.

[8] S. A. Bonke, K. L. Abel, D. A. Hoogeveen, M. Chatti, T. Gengenbach, M. Fournier, L. Spiccia, A. N. Simonov, *ChemPlusChem* **2018**, *83*, 704-710.

[9] M. Chatti, J. L. Gardiner, M. Fournier, B. Johannessen, T. Williams, T. R. Gengenbach, N. Pai, C. Nguyen, D. R. MacFarlane, R. K. Hocking, A. N. Simonov, *Nature Catalysis* **2019**, *2*, 457-465.

[10] Q. Feng, G. Liu, B. Wei, Z. Zhang, H. Li, H. Wang, *Journal of Power Sources* **2017**, *366*, 33-55.

[11] M. Miles, E. Klaus, B. Gunn, J. Locker, W. Serafin, S. Srinivasan, *Electrochimica Acta* **1978**, *23*, 521-526.

[12] a) A. Bard, *Standard potentials in aqueous solution*, Routledge, **2017**; b) C. P. Wilde, M. Zhang, *Journal of Electroanalytical Chemistry* **1992**, *327*, 307-320.

[13] M. Chatti, T. Gengenbach, R. King, L. Spiccia, A. N. Simonov, *Chemistry of Materials* **2017**, *29*, 3092-3099.

[14] D. K. Bediako, C. Costentin, E. C. Jones, D. G. Nocera, J.-M. Savéant, *Journal of the American Chemical Society* **2013**, *135*, 10492-10502.

[15] a) T. Reier, M. Oezaslan, P. Strasser, *Acs Catalysis* **2012**, *2*, 1765-1772; b) R. Berenguer, C. Quijada, E. Morallón, *Electrochimica Acta* **2009**, *54*, 5230-5238; c) A. Grimaud, A. Demortière, M. Saubanère, W. Dachraoui, M. Duchamp, M.-L. Doublet, J.-M. Tarascon, *Nature Energy* **2016**, *2*, 1-10; d) H. N. Nong, L. J. Falling, A. Bergmann, M. Klingenhof, H. P. Tran, C. Spöri, R. Mom, J. Timoshenko, G. Zichittella, A. Knop-Gericke, S. Piccinin, J. Pérez-Ramírez, B. R. Cuenya, R. Schlögl, P. Strasser, D. Teschner, T. E. Jones, *Nature* **2020**, *587*, 408-413.

[16] a) J. S. Mondschein, J. F. Callejas, C. G. Read, J. Y. C. Chen, C. F. Holder, C. K. Badding, R. E. Schaak, *Chemistry of Materials* **2017**, *29*, 950-957; b) A. N. Nikoloski, M. J. Barmi, *Hydrometallurgy* **2013**, *137*, 45-52.

[17] a) A. Hartig-Weiss, M. Miller, H. Beyer, A. Schmitt, A. Siebel, A. T. S. Freiberg, H. A. Gasteiger, H. A. El-Sayed, *ACS Applied Nano Materials* **2020**, *3*, 2185-2196; b) M. Suermann, T. J. Schmidt, F. N. Büchi, *Electrochimica Acta* **2018**, *281*, 466-471.

[18] a) T. Laitinen, J. P. Pohl, *Electrochimica Acta* **1989**, *34*, 377-385; b) D. Pavlov, B. Monahov, *Journal of the Electrochemical Society* **1998**, *145*, 70.

[19] H. S. Oh, H. N. Nong, P. Strasser, *Advanced Functional Materials* **2015**, *25*, 1074-1081.

[20] a) L. G. Bloor, P. I. Molina, M. D. Symes, L. Cronin, *Journal of the American Chemical Society* **2014**, *136*, 3304-3311; b) I. A. Moreno-Hernandez, C. A. MacFarland, C. G. Read, K. M. Papadantonakis, B. S. Brunschwig, N. S. Lewis, *Energy & Environmental Science* **2017**, *10*, 2103-2108; c) M. Huynh, T. Ozel, C. Liu, E. C. Lau, D. G. Nocera, *Chemical science* **2017**, *8*, 4779-4794; d) J. S. Mondschein, K. Kumar, C. F. Holder, K. Seth, H. Kim, R. E. Schaak, *Inorganic chemistry* **2018**, *57*, 6010-6015.